Application of AuNPs embedded in the amyloids fibrils as enhancer in the Laser Induced Breakdown Spectroscopy for the metal quantification in microdroplets

Marcella Dell'Aglio[a,*], Zita Salajkova[b,c], Antonia Mallardi[d], Raffaele Mezzenga[e], Leonie van 't Hag[e], Nicola Cioffi[b], Gerardo Palazzo[b,a], Alessandro De Giacomo[b,a]

a. CNR-NANOTEC, c/o Department of Chemistry, Via Orabona 4, 70126 Bari-Italy
b. University of Bari, Department of Chemistry, Via Orabona 4, 70126 Bari-Italy
c. Central European Institute of Technology (CEITEC), Brno University of Technology, Purkyňova 656/123, 612 00 Brno, Czech Republic
d. CNR-IPCF, c/o Department of Chemistry, Via Orabona 4, 70126 Bari-Italy
e. Department of Health Science and Technology, ETH Zurich, CH-8092 Zurich, Switzerland

Abstract

In this work Nanoparticle Enhanced Laser Induced Breakdown Spectroscopy (NELIBS) has been employed for quantitative metal detection using amyloid fibrils coated with gold nanoparticles as enhancers. Amyloid fibrils represent, from one hand, an extremely interesting system for novel technologies, spacing from water purification to medical applications, and on the other hand, an ideal system for investigating the performance of laser-matter interaction in biological systems. The results obtained in this work show the potentiality of NELIBS for the quantification at sub-ppm (mg/Kg) level of metallic elements (Cr, Pb, Tl and Cd) even in the protein and/or biological environment, employing amyloid fibrils with gold nanoparticles. Moreover, the single-shot measurements reveal the promising use of this technique in applications where high sensitivity and/or limitation in the sample amount are demanded.

Keywords: Nanoparticle enhanced LIBS, amyloids fibrils, gold nanoparticles, micro-droplets, trace elements

1. Introduction

The rapid quantification of trace metals in liquid solutions is of the outmost importance in a large number of applications, including quality control in mechanics, forensics, archeometrics, waste management, environmental and food. In this respect, beyond the traditional analytical tools, LIBS (Laser Induced Breakdown Spectroscopy) represents an interesting alternative and its use for liquid analysis grew dramatically in the last decade [1-4]. LIBS is an analytical technique for elemental chemical analysis based on the optical emission signal of the plasma generated by laser-matter interaction [5]. In the case of sample in condensed phase, hundreds of nanograms of the sample are ablated and then completely atomized and excited in the plasma phase. The amount of any element present in the sample can be quantified by suitable calibration curves, allowing the simultaneous multi-elemental analysis of

major, minor and trace elements. Other advantages of LIBS include the fast response, the possibility of performing analysis without the need of an analytical chamber or sample preparation, a flexible experimental configuration compatible with a small and automatic system [6, 7].
However, the sensitivity usually remains in the range of 1 – 10 ppm (mg/Kg) and this is insufficient for many applications. Furthermore, the sensitivity can be dramatically reduced for samples that are difficult to vaporize. The application of LIBS with organic and biological matrices that are characterized by strong covalent bonding, and inherently made by elements with high ionization energy (carbon, nitrogen, hydrogen and oxygen) [8], is critical. Such samples typically produce very weak plasmas upon laser irradiation.
These issues can be circumvented by means of the Nanoparticle (NP) Enhanced LIBS (NELIBS) [4, 9], which is gaining a growing interest in analytical spectroscopy in the last years. NELIBS is a variant of the LIBS, where plasmonic NPs are deposited *on* or mixed *with* the sample in order to exploit the coupling effect between the electromagnetic field of the incident laser with the induced field in the NP system [9]. The advantage of using NELIBS with respect to the conventional LIBS is that the plasmonic enhancement of the laser electromagnetic field during the ablation stage allows for a better atomization of the ablated sample. This enhances the optical emission signal by orders of magnitude, enabling NELIBS to quantify ppb (μg/Kg) concentrations and significantly decreasing the Limit Of Detection (LOD) of the technique. Another advantage of NELIBS is the possibility to perform analysis by a single laser shot, opening up the possibility to perform analysis of very small sample quantities and to do spatially resolved chemical analysis.
The customary approach for analyzing liquid samples with NELIBS is to deposit the NPs on a solid nonconductive support, put a droplet of sample solution on top, dry it and perform the NELIBS by firing the laser on the position were the NPs and the sample have been deposited [10]. In this frame the sample preparation, i.e. the NP deposition on the substrate, is a crucial step in NELIBS applications and alternative approaches for the nanoparticle deposition is of great interest for developing this technique further [10-14]. To this end, we have herein explored the use of AuNPs synthesised on a template of amyloid fibrils (hereafter AuNPs-amyloids) for obtaining an enhanced NELIBS signal with liquid samples. As a matter of fact, usually the deposition of NPs directly from the colloidal solution requires strong expertise in order to have a reproducible surface concentration, because of the high susceptibility of nanoparticle system to surrounding perturbations. Moreover, the NPs layer deposited on solid substrate suffers of fast aging, so that NELIBS requires to perform the spectroscopic measurement immediately after the sample preparation. On the contrary, if the NPs are immobilized in the amyloid fibrils, they are extremely stable and their distance remains also constant after rough manipulation and the passing time. This allows the deposition of the NPs on movable substrate, like parafilm, that it can be placed on different supports with limited restriction on sample manipulation. At first sight, the employment of amyloids fibrils is a counterintuitive choice because the AuNPs-amyloids have a high concentration of protein which may quench the emission from the analytes (heavy metals atoms). On the other hand, the AuNPs-amyloids display an even distribution of the NPs along the fibrils [15]. An additional advantage is the high viscosity of the sample that could facilitate a uniform deposition by drop casting.
Amyloid fibrils made from food proteins and decorated by inorganic nanoparticles have been employed in many frontier applications, like water detoxification [16],

heterogeneous catalysis [17], materials templating [15] and nutrition applications [18].
The strong affinity of amyloid fibrils for metal ions can potentially be exploited to pre-concentrate the analyte in the case of trace analysis.
NELIBS using amyloid fibrils offers a unique possibility for optimizing laser ablation based techniques for investigating biological systems for trace metal element quantification. As an example, the formation of amyloid fibrils in neurodegenerative diseases due to metal binding [19] has important implications in the diagnostic of such diseases. Additionally amyloid fibrils have found applications in heavy metal ions removal [16], and the quantification of heavy metal ions trapped in the amyloid support may have direct significance in related technologies. Thus, analytical techniques able to detect ppb (μg/Kg) levels of metals, with an extremely small amount of sample, can provide important insights.

2. Materials and methods

2.1 Experimental set-up

The LIBS and NELIBS experimental set-up (Fig. 1) consists of a high energy pulsed laser (Quantel Q-smart 850) with a pulse duration of 6 ns, which is able to deliver enough power >0.5 GW to produce the breakdown, that is focused on the sample with a plano-convex lens of 100 mm focal length. A system of optics was employed to collect the emitted light from the plasma towards a spectroscopic system consisting of a Czerny Turner spectrograph (JY Triax 550) coupled with an ICCD (JY 3000), which was synchronized with the Pockels cell of the laser source with a pulse generator (Stanford DG 535). The acquisition of temporally and spectrally resolved plasma emission can be measured. The experimental parameters employed for these experiments are: laser wavelength = 532 nm, pulse energy of 450 mJ and laser spot size = 2.2±0.2 mm, in order to obtain a fluence = 11.84 J/cm^2. The detection parameters are: delay time from the laser shot = 800 ns, gate width = 10 μs. All the spectra have been acquired in single shot mode. Each measurement was repeated 5 times (on 5 different AuNPs-Amyloids spots in the case of NELIBS) and then averaged. Only 2 – 3 μl of analyte solution is usually employed for a single NELIBS experiment.
A DinoLite optical microscope and ImageJ software have been employed to analyse the AuNPs coatings on different supports and the laser spot size

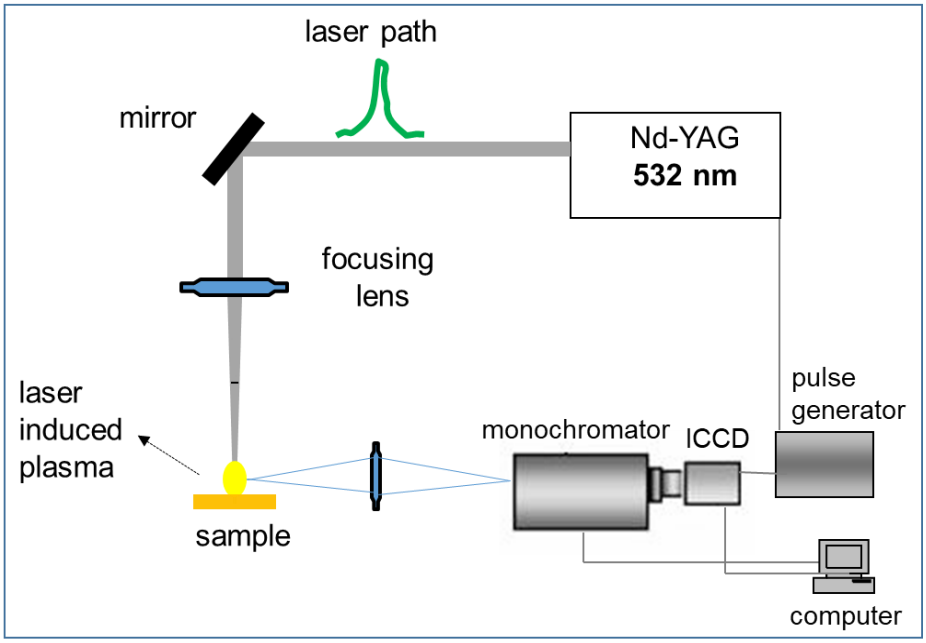

Fig. 1: Experimental set-up for LIBS and NELIBS

Surface Plasmon Resonance (SPR) spectra have been acquired by means of an Agilent 8453 UV-Visible spectrophotometer which uses a photodiode array for simultaneous measurement of the complete ultra-violet to visible light spectrum in less than one second.

TEM analysis was performed with a FEI Tecnai 12 instrument equipped with LaB6 filament operating at 120 kV). Samples were prepared from 1 µL of each AuNPs-amyloid solution on Formvar®-coated Cu grids (300 mesh, Agar Scientific).

2.2 Amyloid fibrils coated with AuNPs

The materials for the preparation of AuNPs reduced onto the amyloid fibrils (hereafter AuNPs-Amyloids) are the following: whey protein isolate (WPI895) was obtained from Fonterra (Palmerston North, New Zealand), containing ≈70% β-lactoglobulin (BLG), ≈20% α-lactoglobulin and ≈5% bovine serum albumin. This was then purified to ≈95% BLG by dialysis [20, 21]. Hydrogen tetrachloroaurate(III) trihydrate ($HAuCl_4$, ACS, 99.99% metal basis) was purchased from ABCR swiss AG (Zug, Switzerland) with 49.5% Au basis. Sodium borohydride (NaBH4) was obtained from Sigma Aldrich (now Merck KGaA, Darmstadt, Germany).

The first step for the preparation of the AuNPs-amyloids was the formation of amyloids fibrils. Whey protein isolate or purified BLG was dissolved in Milli-Q water at 2% w/v and pH 2. This was incubated at 90 °C for 5 hours under stirring. During the incubation amyloid fibrils form due unfolding and hydrolysing of the protein monomer [21]. Fibrils were stored at 4 °C. For all NELIBS experiments purified BLG protein fibrils were used.

The second step was the production of 4 different solutions of AuNPs-Amyloids, in order to obtain solutions with different AuNPs concentrations embedded in the fibrils. Therefore, 1, 2, 3 or 6 mL of 0.09 M chloroauric acid stock solution in Milli-Q water was added to 100 mL 0.2% BLG fibril dispersion followed by mixing. 1, 2, 3 or 6 subsequent additions of 500 µL of 0.074 M $NaBH_4$ in Milli-Q water were added, respectively, to ensure rapid mixing (constant $HAuCl_4$:$NaBH_4$ ratio of 26:11) [22, 15]. Four solutions were therefore prepared with final Au concentrations of 0.17, 0.34, 0.5 and 1 mg/ml, respectively.

2.3 Analytes

In the experiments, 4 analytes have been employed, Cr, Pb, Tl and Cd. The certified standard solutions are the following:

Chromium: $Cr(NO_3)_3$ x $9H_2O$ in 2% HNO_3, standard 1005 ppm (mg/Kg) (Exaxol Italia).

Lead: 1000 mg/L (≈1000 mg/Kg = 1000 ppm) Pb in 2% nitric acid, prepared with $Pb(NO_3)_2$, HNO_3 and water (Fluka TraceCert, SigmaAldrich Switzerland)

Tallium: Tl in 2% HNO_3, standard 1000 ppm (mg/Kg) (Exaxol Italia).

Cadmium: 1000 mg/L (≈1000 mg/Kg = 1000 ppm) Cd in 2% nitric acid, prepared with Cd metal, HNO_3 and water (Fluka TraceCert, SigmaAldrich Switzerland)

2.4 Sample preparation for NELIBS with AuNPs-amyloids

In the case of conventional LIBS experiments, the 2 µl sample was deposited directly on the support and dried by air flow.

The customary approach to analyze liquid samples with NELIBS is to deposit a drop of NPs solution on a solid nonconductive support, let the solvent to evaporate and then put a droplet of sample solution on top of the NP dry deposit, dry it and perform the NELIBS by firing the laser on the position where the sample has been deposited [4, 10]. To achieve a high reproducibility and a high enhancement the spatial distribution of nanoparticles must be as uniform as possible to avoid that different positions on the same target have different NP concentrations.

In this work NELIBS experiment were performed by first depositing a layer of NPs on the substrate by drying 2 µl of a AuNPs-Amyloids solution in an oven for 30 min at 30°C. Subsequently, 2 µl of the metal solution to be analysed was deposited on the NP coating and dried by air flow.

As solid supports, two materials with a different water contact angle (glass and parafilm) have been tested. Depending on the properties of the solid support, the spot size and homogeneity of the AuNP coatings change drastically (See Fig.S1 of the supplementary material). As shown in Fig. S1a, in the case of the hydrophilic glass substrate, the drying of 2 µl of AuNPs-Amyloids leads to a very non-uniform distribution of the NPs. The spreading is very effective leading to a wide coating (about 4 mm in diameter) with a central portion that is depleted in NPs. This region is optically opaque and it coincides with the position where the droplet of the AuNPs-Amyloids solution was initially deposited. The AuNPs formed a ring on the outside of the droplet due to the so-called coffee ring effect. To irradiate the entire NPs coating a laser spot size larger than 4 mm is needed in this case, leading to a strong decreasing of the laser fluence which is unfavourable.

For this reason, we have explored the drop casting on a hydrophobic substrate (i.e. parafilm, plastic paraffin film). In Fig. S1b the coating obtained by drop casting of 2 µl of AuNPs-Amyloids solution on parafilm is shown. The high contact-angle prevents further spreading of the solution so that the final coating has a diameter ≈1.8 mm. A significantly more homogeneous distribution of NPs in the coating was obtained.

For all these reasons, the AuNPs-Amyloids deposited on parafilm substrate have been chosen for the analysis, using a laser spot size of 2.2±0.2 mm (shown in Fig. S1c). The use of a larger spot size with respect to the sample deposition area also avoid eventual border size effects due to the Gaussian shape of the laser pulse. The estimation of laser spot size was performed by firing a single laser shot on an

aluminium target and by measuring the crater size with the optical microscope. Even if this is not the real measurement of the laser spot size and the aluminium target of course undergoes to a different laser matter interaction, it gives the real dimension of the area that the laser will cover during the interaction. As a matter of fact, in Fig. 2b it is demonstrated that all the NPs are removed after the laser shot.
The procedure is illustrated in Fig. 2a. First, 2 µl of AuNPs-Amyloids solution was deposited and then dried in oven at 30°C on a parafilm substrate. Then the parafilm substrate was placed on the glass support in order to perform NELIBS analysis. Then 2 µl of metal solution was deposited on the NPs coating (Fig. 2b); the aqueous solution immediately swells the AuNPs-Amyloids coating leading to an efficient contact among metal ions and AuNPs-Amyloids. In this way all the sample solution drop is fully contained in the area of AuNPs-Amyloids coating. Eventually the metal-AuNPs-Amyloids mixture were further air dried (Fig. 2b) and a laser shot was fired on the dried spot.
A single laser shot is enough to vaporize all the AuNPs-Amyloids coating as shown in Fig. 2b. Finally, as usual in NELIBS experiments, a preliminary spectroscopic investigation on the AuNPs-Amyloids coating, after the sample preparation, is strongly recommended, in order to check contaminants and interferences eventually contained in the matrix.

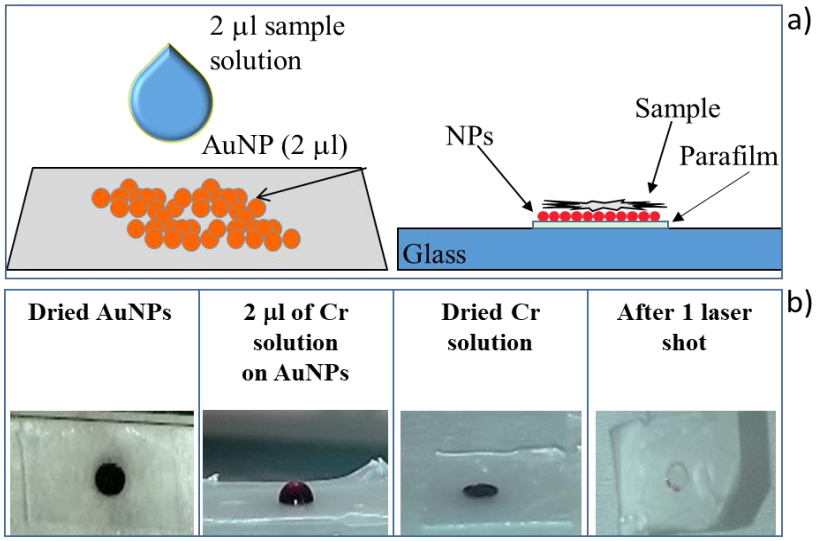

Fig. 2: a) Schematic of the sample preparation and b) images of sample preparation steps before and after the NELIBS measurements

3. Results and discussion

3.1 Arrangement of AuNP on dry AuNPs-Amyloids sample

Homogeneous deposition of the NPs on the substrate is crucial for NELIBS experiments [9, 10]. To achieve a high reproducibility and a high enhancement a couple of constraints must be fulfilled:
i) The spacial distribution of nanoparticles must be as uniform as possible to avoid that different positions on the same target have different NP concentrations.
ii) Maximum enhancement is achieved when an optimal average inter-nanoparticle distance is fulfilled. NPs that are touching each other (as in NP aggregates) behave like an entire metallic surface with a scarce enhancement. Low enhancement is also observed for isolated NPs. It is only when the distance among the NP's edges is less

than or equal to the NP size that synergistic effects lead to a huge LIBS enhancement [9].

Previous work has demonstrated that AuNPs that are synthesised in an amyloid fibril solution are generated from elemental gold nuclei originated by gold ions bound to the fibrils. Accordingly, in ref. [15] high-resolution TEM has revealed evenly distributed AuNPs bound to the fibrils. In order to test the stability of AuNPs-amyloids during the drying where the concentration of the AuNPs-amyloids increases with the water evaporation, we have exposed the AuNPs-Amyloids to different agents (high concentration of divalent cations or diamines) that usually promote the gold NP aggregation in aqueous solutions. The experiments did not show any impact on the AuNP plasmonic peak suggesting that the AuNP remain strongly attached to the fibrils at the BLG amyloid fibril concentration used herein (0.2% w/w) [23], and therefore their uniform interparticle distance was preserved upon drying. TEM images of a representative AuNPs-Amyloid solution (0.34 mg/mL Au, prepared using Whey-protein), deposited on microscopy grids, is shown in Fig. 3. The micrographs show that the NPs are arranged in a linear array along the fibrils over micrometer length-scale. Importantly, there is only limited evidence of inter-NP contact and the average edge to edge distance is below ten nanometers. Therefore, this kind of sample effectively fulfils the main conditions to achieve the electromagnetic field enhancement. Since the theory suggests that the size distribution of the NPs, whenever the previous condition of an even distribution is abided, does not significantly affect the NELIBS effect [9]. The actual size of the AuNP is of marginal importance when their inter-particle distance is optimized.

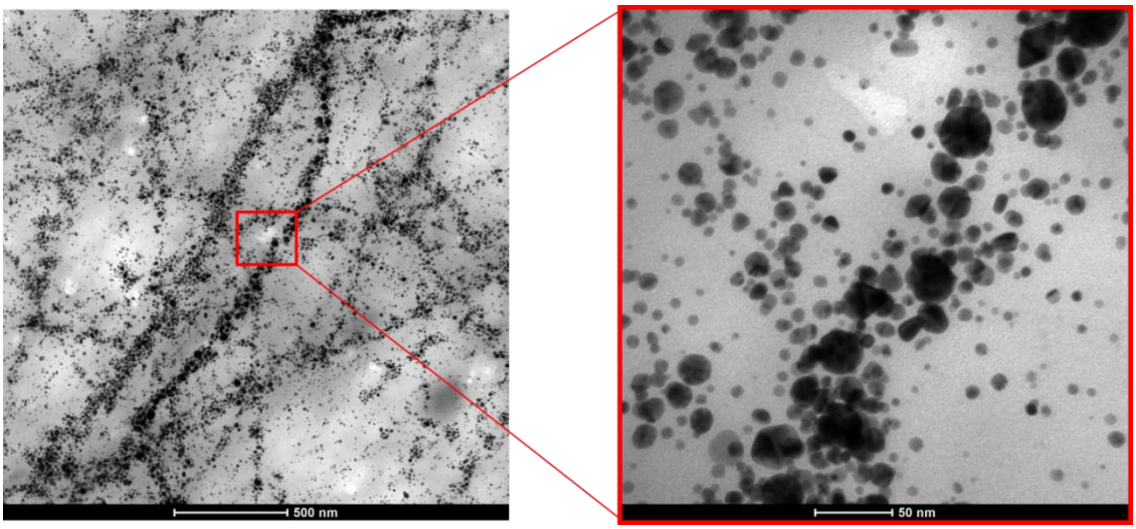

Fig. 3: Representative low resolution TEM of AuNPs-Amyloids deposited on microscopy grids (solution *b* of Table 1)

The TEM micrographs shown in Fig. 3 show that the AuNPs-Amyloids are interesting candidates as enhancer in NELIBS quantification of different metals ions. We show this for Cr, Pb, Tl and Cd solutions herein.

3.2. LIBS and NELIBS Emission Spectra on amyloids fibrils.

The plasma emission spectra detection has been accomplished in single shot mode for both LIBS and NELIBS experiments. A set of certified Chromium solutions have been analysed in order to investigate the general emission spectrum features of the NELIBS.

In Fig. 4 the emission spectra (in the spectral region of Cr I emission line) acquired with normal LIBS (i.e. in the absence of metallic NPs) and by NELIBS (i.e. with AuNPs) on amyloid fibrils are shown.

In particular, panel Fig. 4a compares the LIBS and NELIBS emission spectra obtained in the absence of any analyte (chromium in this instance). The LIBS spectra obtained by firing the laser on the glass slide (red dashed spectrum) and on parafilm supported on a glass slide (blue dashed spectrum) are compared with the NELIBS emission spectrum acquired by firing the laser on a layer of AuNPs-amyloids (black curve) on parafilm supported on the glass slide. In the first two cases (LIBS experiments), no emission lines were observed suggesting no stable plasma was induced on the substrate. On the contrary, the emission spectrum of AuNPs-amyloids deposited on parafilm (NELIBS experiment) clearly showed the expected structured emission lines: Au I and C_2 emission peaks were clearly visible. The C_2 band is due to a recombination of excited C atoms and ions during the plasma expansion and are combined with intense CN bands (see Fig. S2 of supplementary material) [24]. The presence of the carbon signal can be explained by the efficient ablation of protein molecules, although we cannot exclude a partial contribution from the parafilm substrate (the prominence of the carbon signals is either way ascribed to the NELIBS effect [9,25]). The Ca I and Mg I lines are ascribed to the presence of these ions in the whey that was used to prepare the BLG amyloid fibrils and are not considered. The emission signal of each element present in the dried sample is dramatically enhanced by the AuNPs, notwithstanding the simultaneous presence of the BLG protein. Fig. 4b and c show the NELIBS and LIBS emission spectra obtained in the presence of chromium, at the same concentration, by employing AuNPs-amyloids and amyloid fibrils, respectively. For the NELIBS experiment the active substrate is formed by AuNPs-amyloids dried on parafilm, while for the LIBS blank experiment the same amount of amyloid fibril solution, without AuNPs, (the absorbance spectrum is reported in supplementary material Fig. S3) was dried on parafilm. In both cases, 2 μl of 0.1 ppm $Cr(NO_3)_3$ solution was deposited on the amyloid fibrils. It was noticed that in the presence of AuNPs (NELIBS, Fig. 4b), the carbon molecular signal is significantly enhanced compared to the LIBS experiment (Fig. 4c). This intensity increase of the emission bands reflects the efficient atomization of the amyloid fibrils in the presence of the AuNPs during NELIBS. In this frame, the NELIBS effect results in the more efficient atomization, releasing and excitation of the metallic elements adsorbed onto the fibrils (because of the NPs synthesis and further sample drop deposition) into the plasma phase. Accordingly, the sensitive detection of the analyte as well as an increased signal for the endogenous magnesium and calcium ions can be obtained by going from the LIBS to the NELIBS experiments.

In the insets of Fig. 4 the spectral region for the Cr detection is enlarged in order to show the appearance of the three Cr I emission lines in NELIBS, which were not detected in the LIBS spectrum.

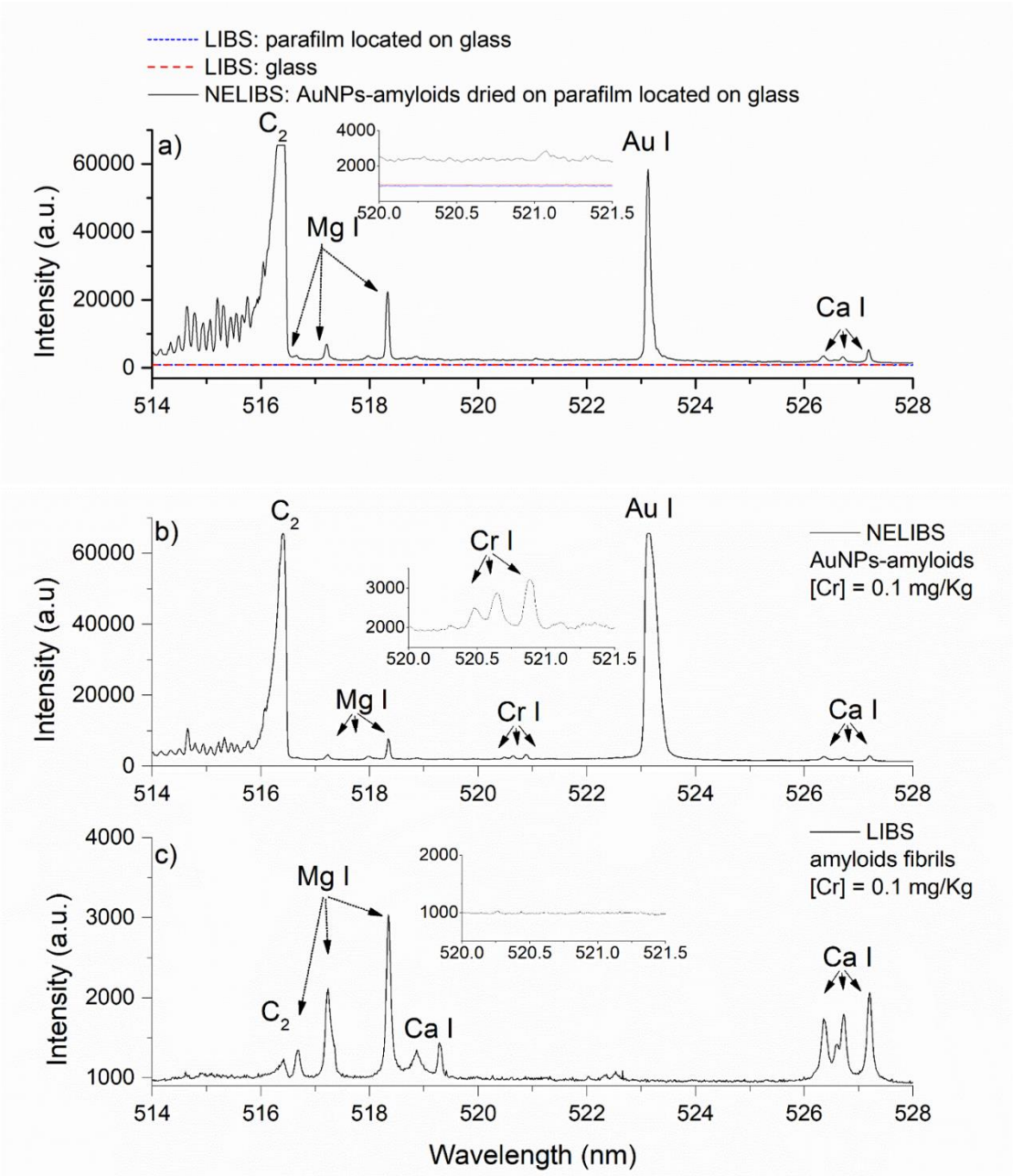

Fig. 4: Plasma emission spectra: a) LIBS on parafilm located on glass, LIBS on glass and NELIBS on AuNPs-amyloids dried on parafilm located on glass; b) NELIBS of $Cr(NO_3)_3$ solution on AuNPs-amyloids and c) LIBS of $Cr(NO_3)_3$ solution on amyloids fibrils. The Cr concentration was 0.1 mg/Kg and the sample volume was 2 µl. The insets report the enlargement of the spectral region of the emission lines of Cr. All the emission spectra are acquired with the same experimental conditions. The AuNPs amyloids employed for these experiments was the solution *b*, prepared with purified BLG fibers and 0.34 mg/mL Au, as reported in Table 1.

3.3 Effect of AuNP concentration in Amyloid fibrils on NELIBS signal.

A critical NP concentration per surface area is necessary to obtain the optimal NELIBS signal enhancement [9, 26]. For this reason, solutions with different AuNP concentrations have been investigated herein.

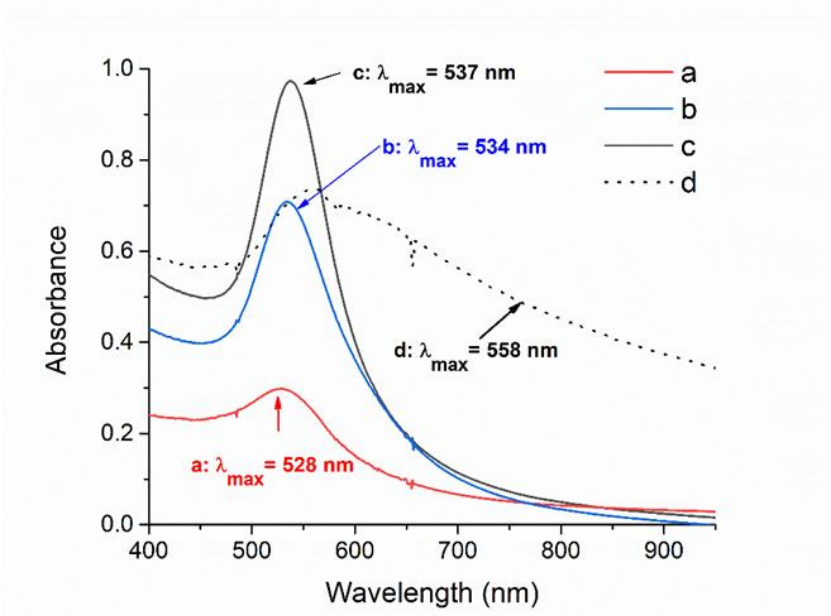

Fig. 5: SPR spectra of different AuNPs-amyloid solutions with characteristics as reported in Table 1. The solutions *a*, *b* and *c* were diluted 1:10 with amyloid fibrils solution (0.2% w/w β-lactoglobulin), the solution *d* were diluted 1:50.

Table 1 AuNPs-amyloids solutions characterized from SPR spectra in Fig. 5. The concentration of Au employed for the NPs synthesis is compared with the ones calculated from the AuNPs concentration obtained from the SPR spectra. NP diameter (2R) with relative error and concentration of AuNPs are also calculated from the SPR spectra [27, 28], as reported in the text. The AuNPs surface density is the number of AuNPs per unit surface.

	[Au] from $HAuCl_4$ (mg/ml)	λ_{max} (nm)	Abs_{450nm}	$Abs_{\lambda max}$	[Au] calculated from SPR (mg/ml)	2R calculated from SPR (nm)	[AuNP] Calculated from SPR (nM)	Surface Density (number of AuNPs/m^2)
a	0.17	528	2.3	2.9	0.17	6±2	162	$7.6 \cdot 10^{16}$
b	0.34	534	3.9	7.1	0.34	18±2	10	$4.7 \cdot 10^{15}$
c	0.50	537	4.9	9.7	0.44	26±3	4	$1.9 \cdot 10^{15}$
d	1.00	558	-	11.95	0.45	80±5	0.14	$6.6 \cdot 10^{13}$

In Fig. 5 the surface resonance spectra of four AuNPs-amyloids samples synthesized from different $HAuCl_4$ concentrations are shown. All the samples showed a SPR maximum characteristic of metallic nanoparticles. For each solution, the wavelength at which the maximum of the surface plasmon resonance (SPR) is located (λ_{max}) is reported in Table 1, as well as the absorbance at 450 nm and at λ_{max}. In addition, Table 1 reports an estimation of the NP diameter (2R) and concentration, [AuNP]. For the solutions *a*, *b* and *c*,the diameters have been estimated according to the relation between the absorbance at λ_{max} and the absorbance at λ_{450} as function of size, instead the concentrations have been estimated with the Lambert Beer law applied to the absorbance at λ_{max} . The employed calibration curves have been obtained elsewhere, in the case of AuNPs in water [27] for AuNPs with diameter lesser than 35 nm [28]. The refractive index of the medium strongly impacts the position of the SPR peak, therefore the use of a calibration curve measured with water as solvent as a measure for a NP dispersion in a protein solution must be carefully considered. However, the

calculation successfully captured the order of magnitude of the NP size (2R) and concentration [AuNP] as confirmed by comparing the Au concentration (mg/ml Au from $HAuCl_4$) used in the AuNP synthesis (Table 1) with the Au concentration calculated by the SPR spectra.

For the AuNPs-amyloids with an overall gold content ≤0.5 mg/ml (solutions *a*, *b* and *c*) the metallic gold accounts for the overall content. In the case of the highest initial $HAuCl_4$ concentration (solution *d*) the system phase separates into a viscous lower phase rich in AuNPs (its colour is burgundy) and a transparent upper phase. In FigS4 of the supplementary material, the absorbance spectra of the two phases are compared. The spectrum of the lower phase is also shown in Figure 5 and clearly shows a long wavelength tail indicative of AuNPs aggregation. However, a rough estimation of the main AuNP size can still be performed in first approximation with the de-convolution of the SPR band in two peaks: one is ascribed to the spherical AuNPs and the other to the aggregate state (see FigS5) . Then, as reported in [28], when the size of AuNPs is bigger than 35 nm, that is the case of solution *d*, a direct correlation between λ_{max} and size can be employed for the size evaluation, starting from a calibration curve of the λ_{max} as function of AuNPs size. In the supplementary material the calibration curves useful for these calculations is reported (table S1). This approach indicates the presence, in the lower phase, of large individual particles (≈80 nm in diameter) coexisting with clusters that are responsible of the long-wavelength tail.

All these AuNPs-amyloids samples (including the Au-rich lower phase of sample *d*) have been tested as NELIBS matrix for the determination of the chromium concentration in water. For each AuNPs-amyloids sample, a calibration curve was obtained by measuring the NELIBS emission intensity as a function of the chromium content within 2 μl solution of $Cr(NO_3)_3$ (0.01-0.2 ppm (mg/Kg) concentration range). In Fig. 6a, Cr calibration curves acquired with different AuNPs-amyloids samples are presented. For all samples the NELIBS intensity increases linearly with the chromium content.

The best results, from the analytical point of view, were obtained when AuNPs-amyloids solutions *b* and *c* were employed. For solution *a* the number of AuNPs per surface unit was larger than for solutions *b* and *c*. It can be observed in Fig. 6a, however, that the obtained Cr signal at each concentration was lower and the Cr calibration curve did not result in a good fit (R^2 = 0.82). We suggest that in solution *a* the distance between the NPs useful for the NELIBS effect was not optimal. Even though it has the largest number of NPs, it also has the smallest AuNPs and lowest concentration of Au. When dealing with smaller NPs, a smaller distance between the particles is required for the electromagnetic field enhancement and the preparation of the sample is more difficult as it requires a significantly larger number of particles [26]. On the other hand, solution *d*, which contains aggregates, also showed a clear NELIBS signal. Nevertheless, this signal was smaller than that obtained with the solution with similar concentration of Au where the NPs aggregation did not occur (solution *c*).

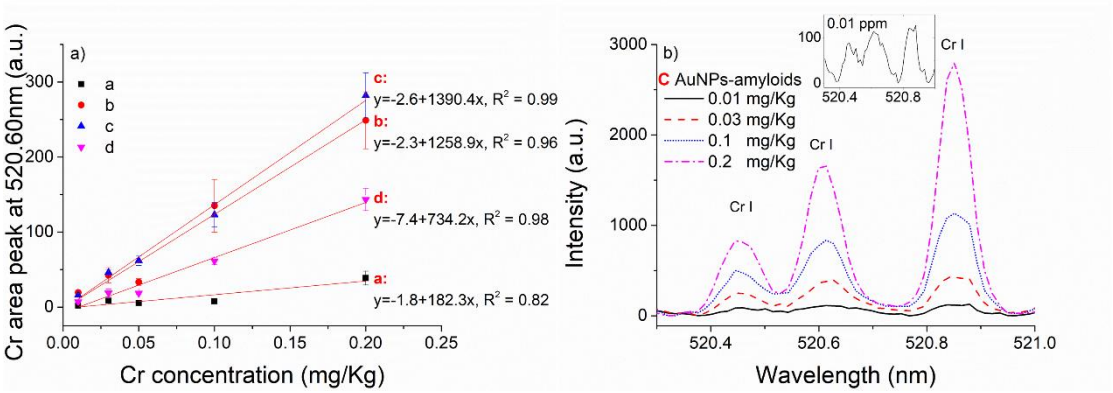

Fig. 6: a) NELIBS Cr calibration curves by using different AuNPs-solutions (reported in Table 1). Relative errors are also reported for each intensity. b) Cr I emission lines acquired by using AuNPs-amyloids solution *c* at different Cr concentrations: 0.01, 0.03, 0.1, 0.2 ppm, respectively.

3.4 NELIBS for the analysis of metals using AuNPs-Amyloid fibrils.

Since the best calibration curve, in terms of reproducibility and signal enhancement, for Cr was obtained with solution *c*, this solution was selected to perform NELIBS on the other analytes.

In this work, Cr, Pb, Tl and Cd elements have been measured by employing only 2 or 3 μl of solution of each element. By starting from certified mother solutions, different concentrations have been used for each analyte in order to build a calibration curve and therefore estimating the LOD for each element. The chosen emission peaks for the analytes are the following: Cr I at 520.60 nm, Pb I at 405.78 nm, Cd I at 346.6. In Fig.S7, S8 and S9 of the Supplementary material the emission spectra in the regions useful for the Pb, Tl and Cd detection are shown. In Table 2 the spectroscopic data of the chosen emission lines for each element, as well as the calculated LODs, are reported. Since the employed volume for the single analysis is known, 2 μl for Cr and 3 μl for Tl, Cd and Pb, the minimum mass of the element can be also evaluated, as reported in Table 2.

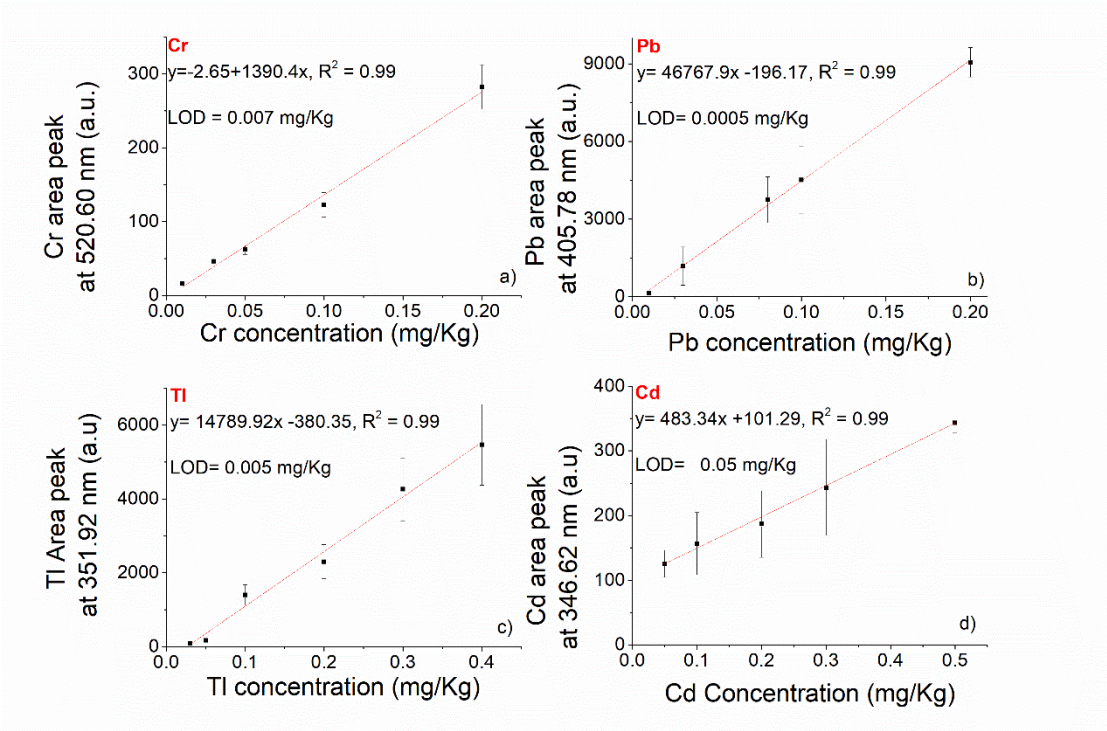

Fig. 7: Calibration curves of Cr, Pb, Tl and Cd. The linear fit with the R-square, the LOD for each element and relative errors for each intensity are also reported.

Table 2: Spectroscopic data of the emission lines employed for the analysis and calculated LOD

Element	λ (nm)	E_i (cm^{-1})	E_u (cm^{-1})	LOD (μg/kg)	Absolute LOD (pg) for single analysis
Cr I	520.60	7593.15	26796.27	7	14
Pb I	405.78	10650.33	35 87.22	0.5	1.5
Tl I	351.92	7792.70	36199.90	5	15
Cd I	346.62	30656.09	59497.87	50	150

The limit of detection for each sample has been calculated by LOD = 3 σ/*m*, where σ is the standard deviation of the background measured in a region of the spectrum where no emissions can be revealed and *m* is the slope of the calibration curve [29]. The calibration curves reported in Fig. 7 were obtained by plotting the areas of the emission peaks as a function of the concentration of the employed analyte. The maximum peak intensity as a function of the analyte concentration has further been employed for the determination of the LOD [29].

It is clearly visible in Fig. 7 how all the investigated elements can be detected at sub-ppm (mg/Kg) (e.g. Cd) down to ppb (μg/Kg) concentrations using the AuNPs-amyloids fibrils .

Samples with Cd showed the least accurate calibration curve (in terms of slope and intercept) and highest LOD with respect to the other elements. This is due to the high energy of the emission line used in this experiment (Table 2). For the LIBS analysis of Cd traces, the emission line at 228.8 nm is usually employed. Since this is a resonance transition and it has the potential to significantly decrease the LOD. In the experiment used, however, the detector is not enabled for deep UV detection. Nevertheless, it demonstrates that the laser-matter interaction mediated by NPs

allowed for the detection of the emission lines with a very high upper level even though the analysis is performed in an organic environment.
These results open up the possibility of analysing solutions containing sub-ppm (mg/Kg) levels of metallic elements and proteins when analysis of small sample volumes is required.

4. Conclusions

In this work, the employment of amyloid fibrils coated with gold nanoparticles has been tested as enhancers of LIBS technique for quantitative metal detection. It shows that, despite the significant presence of proteins that usually produce a strong quenching of plasma, the presence of an ordered array of AuNPs enables a very good plasma analysis by laser ablation based techniques such as LIBS. This study shows that NELIBS allows for efficient atomization of the organic sample during the laser sampling and result in the detection of elements in the presence of amyloid fibrils. The metal analytes probably also bind to the amyloid fibrils on the substrate. In this frame, NELIBS can be employed for the determination of trace metallic elements (sub-ppm (mg/Kg) and for some elements down to sub-ppb (μg/Kg) concentrations) in solution using amyloid protein fibril systems by consuming significantly lower sample volumes (2 – 3 μl).

Acknowledgments:
One of the authors, Z. Salajková, would like to acknowledge the financial support by the Ministry of Education, Youth and Sports of the Czech Republic under the project CEITEC 2020 (LQ1601).

References

[1] X. Y. Yang, Z. Q. Hao, C. M. Li, J. M. Li, R. X. Yi, M. Shen, K. H. Li, L. B. Guo, X. Y. Li, Y. F. Lu, and X. Y. Zeng, "Sensitive determinations of Cu, Pb, Cd, and Cr elements in aqueous solutions using chemical replacement combined with surface-enhanced laser-induced breakdown spectroscopy," Opt. Express 24, 2016, 13410-13417

[2] N. Aras, S. Yalcin, Investigating silicon wafer based substrates for dried-droplet analysis by Laser-Induced Breakdown Spectroscopy, Spectrochimica Acta B, 2019, 152, 84-92.

[3] Dongsun Bae, Sang-Ho Nam, Song-Hee Han, Jonghyun Yoo, Yonghoon Lee, Spreading a water droplet on the laser-patterned silicon wafer substrate for surface-enhanced laser-induced breakdown spectroscopy, Spectrochimica Acta B, 2015, 113, 70-78.

[4] A. De Giacomo, C. Koral, G. Valenza, R. Gaudiuso, M. Dell'Aglio, Nanoparticle Enhanced Laser-Induced Breakdown Spectroscopy for Microdrop Analysis at subppm Level, Analytical Chemistry, 2016, 88 (10), 5251-5257.

[5] L.J. Radziemski, D.A. Cremers (Eds.), Laser-induced plasma and applications, Marcel Dekker, New York, 1989.

[6] D.W. Hahn, N. Omenetto , Laser-induced breakdown spectroscopy (LIBS), part II: review of instrumental and methodological approaches to material analysis and applications to different fields, Appl Spectrosc. 2012, 66(4), 347-419

[7] K. Rifai, F. Doucet, L. Ozcan, F. Vidal, LIBS core imaging at kHz speed: Paving the way for real-time geochemical applications, Spectrochimica Acta B, 2018, 50, 43-48

[8] L. Mercadier, J. Hermann, C. Grisolia, A. Semerok, Diagnostics of nonuniform plasmas for elemental analysis via laser-induced breakdown spectroscopy: Demonstration on carbon-based materials, Journal of Analytical Atomic Spectrometry, 2013, 28 (9), 1446-1455.

[9] M. Dell'Aglio, R. Alrifai, A. De Giacomo , Nanoparticle Enhanced Laser Induced Breakdown Spectroscopy (NELIBS), a first review. Spectrochimica Acta B, 2018, 148 105–112

[10] S.C. Jantzi, V. Motto-Ros, V., F. Trichard, Y. Markushin, N. Melikechi, A. De Giacomo, Sample treatment and preparation for laser-induced breakdown spectroscopy Spectrochimica Acta B 2016, 115, 52-63.

[11] C. Sánchez-Aké, T. García-Fernández, J.L. Benítez, M.B. de la Mora, M. Villagrán-Muniz, Intensity enhancement of LIBS of glass by using Au thin films and nanoparticles, Spectrochimica Acta B, 2018, 146, 77-83

[12] Rusak, D.A., Anthony, T.P., Bell, Z.T. Note: A novel technique for analysis of aqueous solutions by laser-induced breakdown spectroscopy, Review of Scientific Instruments, 2015, 86 (11), 116106

[13] Xu, W., Lin, Q., Niu, G., Qi, S., Duan, Y. Emission enhancement of laser-induced breakdown spectroscopy for aqueous sample analysis based on Au nanoparticles and solid-phase substrate, Applied Optics, 2016, 55 (24), 6706-6712.

[14] Dong, D., Jiao, L., Du, X., Zhao, C., Ultrasensitive nanoparticle enhanced laser-induced breakdown spectroscopy using a super-hydrophobic substrate coupled with magnetic confinement, Chemical Communications, 2017, 53 (33), 4546-4549.

[15] Nyström, G.; Fernández-Ronco, M. P.; Bolisetty, S.; Mazzotti, M.; Mezzenga, R. Amyloid Templated Gold Aerogels, Adv. Mater. 2015, 28 (3), 472–478.

[16] Sreenath Bolisetty and Raffaele Mezzenga, Amyloid–carbon hybrid membranes for universal water purification, Nature Nanotechnology, 2016, 11, 365-372

[17] Nanda, J., Biswas, A., Adhikari, B. & Banerjee, A. A gel-based trihybrid system containing nanofibers, nanosheets, and nanoparticles: modulation of the rheological property and catalysis. Angew. Chem. Int. Ed., 2013, 52, 5041–5045

[18] Yi Shen, Lidija Posavec, Sreenath Bolisetty, Florentine M Hilty, Gustav Nyström, Joachim Kohlbrecher, Monika Hilbe, Antonella Rossi, Jeannine Baumgartner, Michael B Zimmermann and Raffaele Mezzenga, Amyloid fibril systems reduce, stabilize and deliver bioavailable nanosized iron, Nature Nanotechnology, 2017, 12, 642-647[19] Dorothea Strozyk and Ashley I. Bush, The Role of Metal Ions in Neurology. An Introduction, in Neurodegenerative Diseases and Metal Ions, Editor(s): Astrid Sigel Helmut Sigel Roland K. O. Sigel, 2006 John Wiley & Sons, Ltd

[20] Jung, J.-M.; Savin, G.; Pouzot, M.; Schmitt, C.; Mezzenga, R. Structure of Heat-Induced β-Lactoglobulin Aggregates and Their Complexes with Sodium-Dodecyl Sulfate. Biomacromolecules 2008, 9 (9), 2477–2486.

[21] Jung, J.-M.; Mezzenga, R. Liquid Crystalline Phase Behavior of Protein Fibers in Water: Experiments versus Theory. Langmuir 2010, 26 (1), 504–514.

[22] Bolisetty, S.; Arcari, M.; Adamcik, J.; Mezzenga, R. Hybrid Amyloid Membranes for Continuous Flow Catalysis. Langmuir 2015, 31 (51), 13867–13873.

[23] Sreenath Bolisetty, Ludger Harnau, Jin-mi Jung, and Raffaele Mezzenga, Gelation, Phase Behavior, and Dynamics of β-Lactoglobulin Amyloid Fibrils at Varying Concentrations and Ionic Strengths, Biomacromolecules 2012 13 (10), 3241-3252

[24] Ángel Fernández-Bravo, Tomás Delgado, Patricia Lucena, J. Javier Laserna, CN emission spectroscopy study of carbon plasma in nitrogen environment Vibrational emission analysis of the CN molecules in laser-induced breakdown spectroscopy of organic compounds, Spectrochimica Acta B, 2013, 89, 77–83

[25] Z. Abdel-Salam, Sh.M.I. Alexeree, M.A. Harith, Utilizing biosynthesized nano-enhanced laser-induced breakdown spectroscopy for proteins estimation in canned tuna, Spectrochimica Acta B, 2018, 149, 112-117,

[26] A. De Giacomo, M. Dell'Aglio, R. Gaudiuso, C. Koral, G. Valenza, Perspective on the use of nanoparticles to improve LIBS analytical performance: Nanoparticle enhanced laser induced breakdown spectroscopy (NELIBS), Journal of Analytical Atomic Spectrometry, 2016, 31 (8), 1566-1573.

[27] M. Dell'Aglio, V. Mangini, G. Valenza, O. De Pascale, A. De Stradis, G. Natile, F. Arnesano, A. De Giacomo, Silver and gold nanoparticles produced by pulsed laser ablation in liquid to investigate their interaction with Ubiquitin, Applied Surface Science, 2016, 374, 297-304.

[28] W. Haiss, N.T. K. Thanh, J. Aveyard, and D. G. Fernig, Determination of Size and Concentration of Gold Nanoparticles from UV-Vis Spectra, Anal. Chem., 2007, 79, 4215-4221.

[29] D. W. Hahn, N. Omenetto, Laser-Induced Breakdown Spectroscopy (LIBS), Part II: Review of Instrumental and Methodological Approaches to Material Analysis and Applications to Different Fields, Applied Spectroscopy, 2012, 66 (4),

Supplementary material

Application of AuNPs embedded in the amyloids fibrils as enhancer in the Laser Induced Breakdown Spectroscopy for the metal quantification in microdroplets

Marcella Dell'Aglio[a,*], Zita Salajkova[b,c], Antonia Mallardi[d], Raffaele Mezzenga[e], Leonie van 't Hag[e], Nicola Cioffi[b], Gerardo Palazzo[b,a], Alessandro De Giacomo[b,a]

a. CNR-NANOTEC, c/o Department of Chemistry, Via Orabona 4, 70126 Bari-Italy
b. University of Bari, Department of Chemistry, Via Orabona 4, 70126 Bari-Italy
c. Central European Institute of Technology (CEITEC), Brno University of Technology, Purkyňova 656/123, 612 00 Brno, Czech Republic
d. CNR-IPCF, c/o Department of Chemistry, Via Orabona 4, 70126 Bari-Italy
e. Department of Health Science and Technology, ETH Zurich, CH-8092 Zurich, Switzerland

---

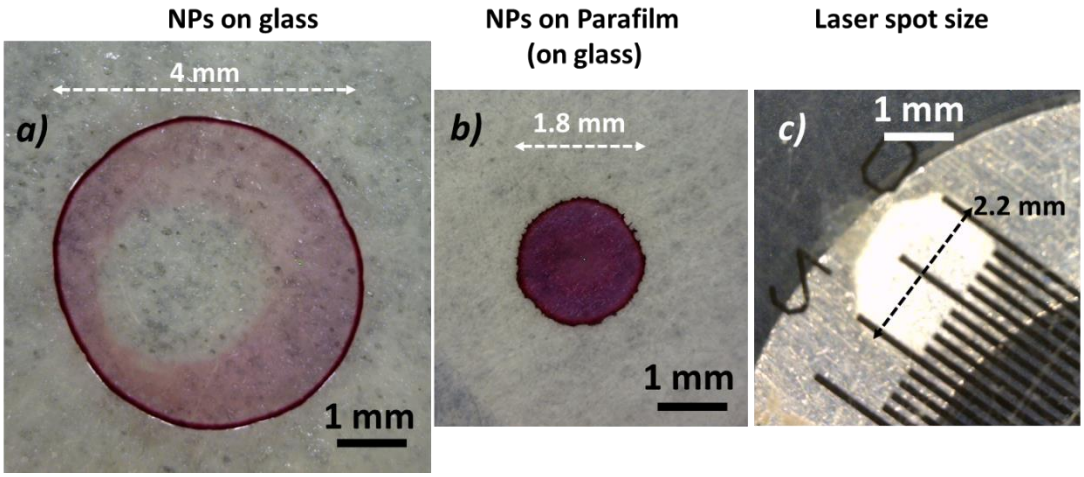

Fig.S1 AuNPs-amyloids deposition on a) glass and b) parafilm. c) laser spot size. The measures are performed with DinoLite microscope and analysed with ImageJ software.

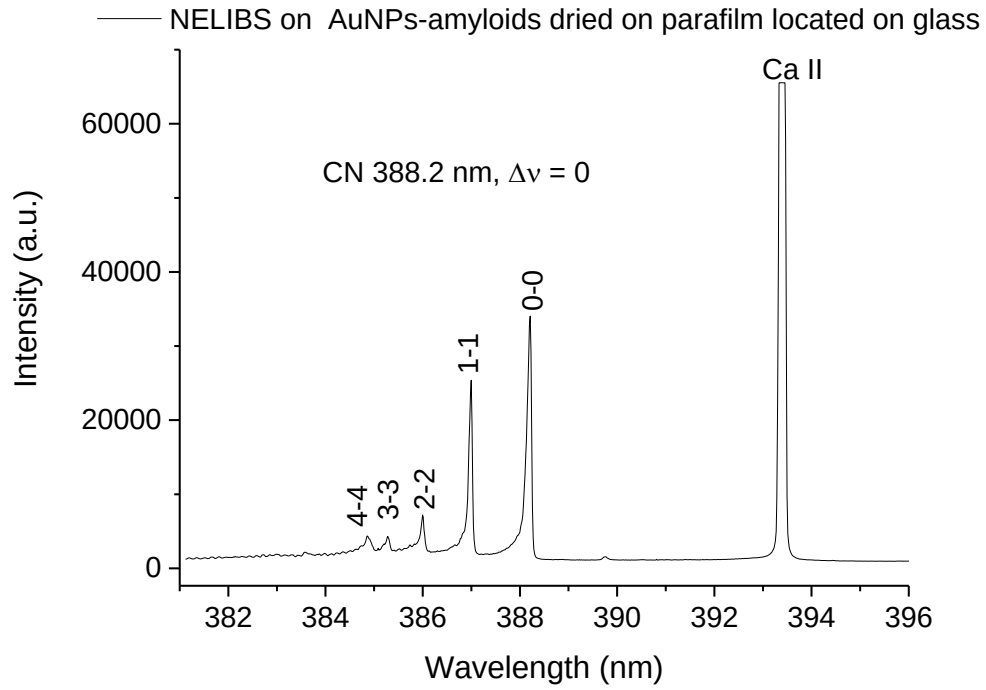

Fig.S2 Emission spectrum during NELIBS on AuNPs-amyloids (dried on parafilm located on glass), acquired in the spectral region of CN vibrational modes. The experimental conditions of this experiment were different with respect to those reported in the main paper: laser energy and gain of ICCD were reduced in order to avoid peaks saturation. (λ_{laser} = 532 nm, E_{laser}= 400 mJ, laser spot size = 2.2±0.2 mm, fluence = 10.5 J/cm^2; delay time = 800 ns, gate width = 10 μs, acquisition in single shot mode).

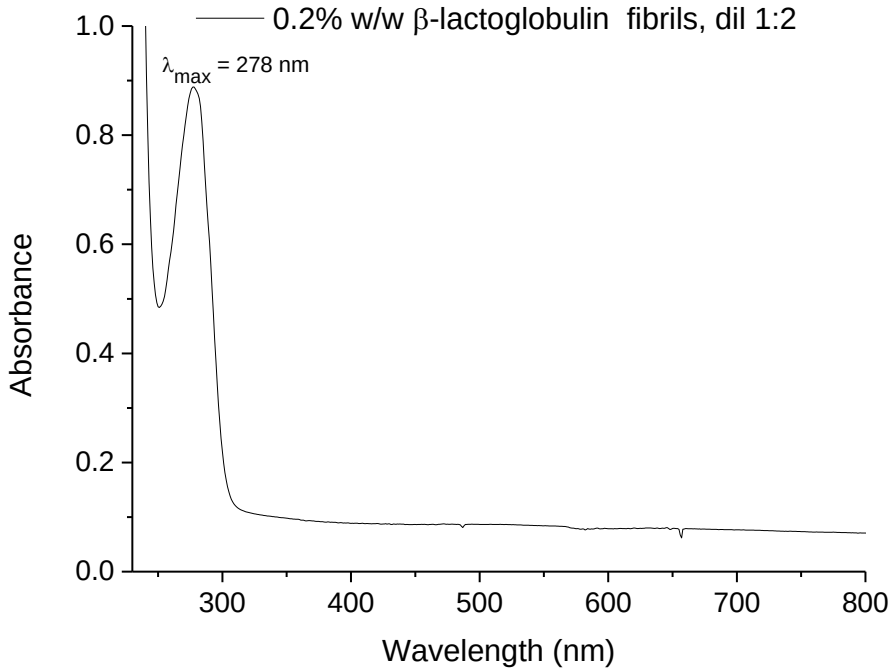

Fig.S3 Absorbance spectrum of 0.2% w/w β-lactoglobulin fibrils (BLG), diluted 1:2 with MQ-water

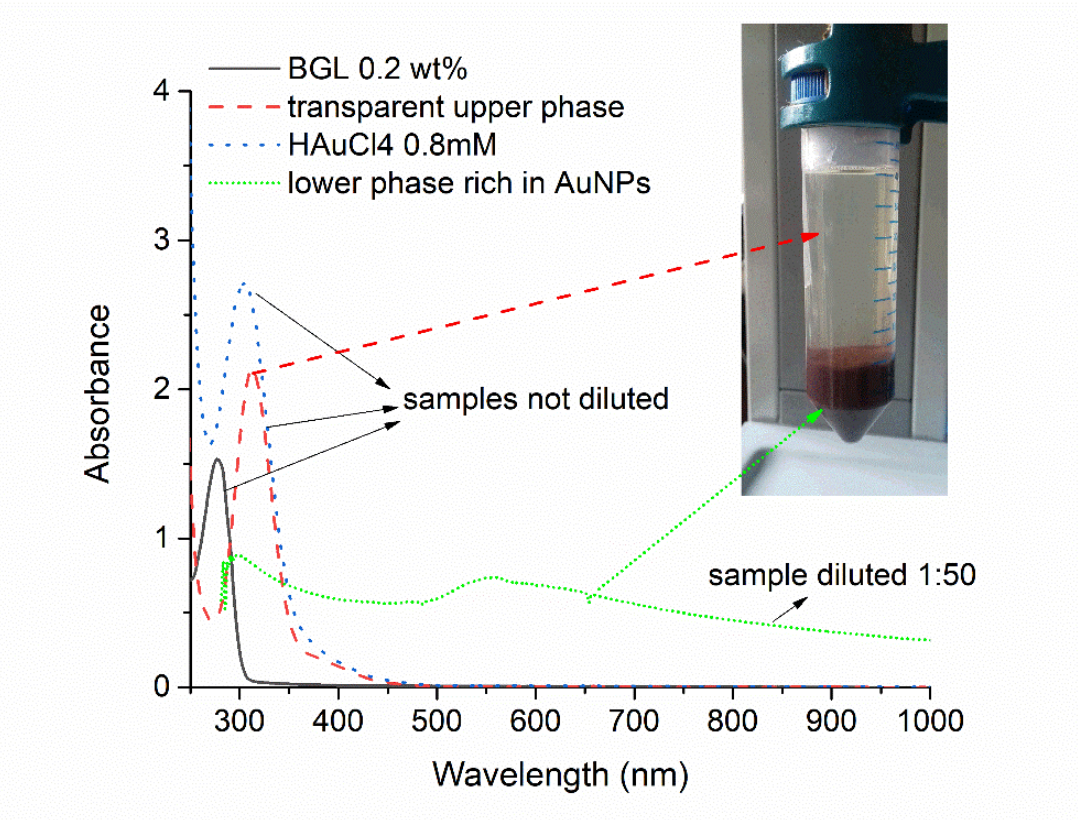

Fig. S4 SPR spectra of AuNPs-amyloids (solution *d*) obtained with the highest initial $HAuCl_4$ concentration (1 mg/ml). The system phase separates into a viscous lower phase rich in AuNPs and a transparent upper phase: green short dot and red dash lines, respectively. For a comparison, the absorbance spectra of BLG 0.2 wt% and of $HAuCl_4$ 0.8 mg/ml are also reported, black solid and blue dot lines, respectively.

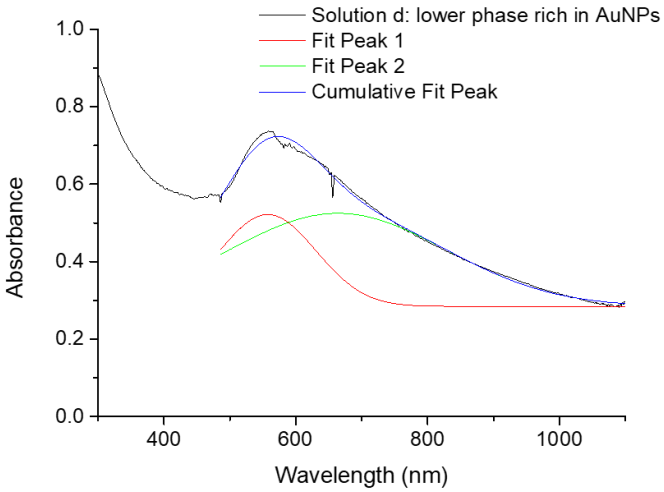

Model	Gauss		
Equation	y=y0 + (A/(w*sqrt(PI/2)))*exp(-2*((x-xc)/w)^2)		
Reduced Chi-Sqr	7.40108E-5		
Adj. R-Square	0.99655		
		Value	Standard Error
Peak1(F)	y0	0.28432	0.00116
Peak1(F)	xc	557.56448	0
Peak1(F)	w	146.13747	2.26798
Peak1(F)	A	43.44305	1.69487
Peak1(F)	sigma	73.06874	1.13399
Peak1(F)	FWHM	172.06372	2.67035
Peak1(F)	Height	0.23719	0.00599
Peak2(F)	y0	0.28432	0.00116
Peak2(F)	xc	663.74769	3.41856
Peak2(F)	w	330	0
Peak2(F)	A	99.39907	1.46897
Peak2(F)	sigma	165	0
Peak2(F)	FWHM	388.54531	0
Peak2(F)	Height	0.24033	0.00355

Fig. S5 : De-convolution of the AuNPs-amyloids (lower phase rich in AuNPs, solution *d*) SPR band in two peaks, one ascribed to the spherical AuNPs size and the other to an aggregate state.

Table S1

1) Curve fitting of λ_{max} VS d d=particle diameter (nm) λ_{max} = wavelength at maximum of absorbance (nm)	$\lambda_{max} = \lambda_0 + L_1 \exp(L_2 d)$, eq.1 with R^2=0.999 *where λ_0 = 508.04 nm, L_1=11.29, L_2=0.018*
2) Curve fitting of $A_{\lambda max}$ VS C_{AuNPs} C_{AuNPs}=AuNPs Concentration (mol of NPs /l) $A_{\lambda max}$ = maximum of absorbance = lε C_{AuNPs} (path length*extinction coefficient*concentration)	A_{max}=-0.0033+8.23*10^{10} C_{AuNPs} eq.2 with R^2=0.999

Eq1 is the fitting of the calibration curve, wavelength at the maximum of absorbance, λ_{max}, as function of particle diameter, d, valids for particle diameters ranging from 35 to 100 nm. AuNPs in 2 mM citrate purchased from Sigma Aldrich (0.06 g L^{-1}) are employed. The procedure is the same of that reported in [28].
Eq. 2 is the fitting of the calibration curve, absorbance at the maximum wavelength as function of AuNPs concentration in terms of mole of NPs/liter (M), at fixed diameter of 80 nm. AuNPs of 80 nm particle size in 2 mM citrate purchased from Sigma Aldrich (with concentration ranging from 0.06 g $L^{-1}$to 0.04 g L^{-1}) are employed. The Lambert Beer law is finally applied to the calibration curve of the absorbance at λ_{max} for the unknown concentration.

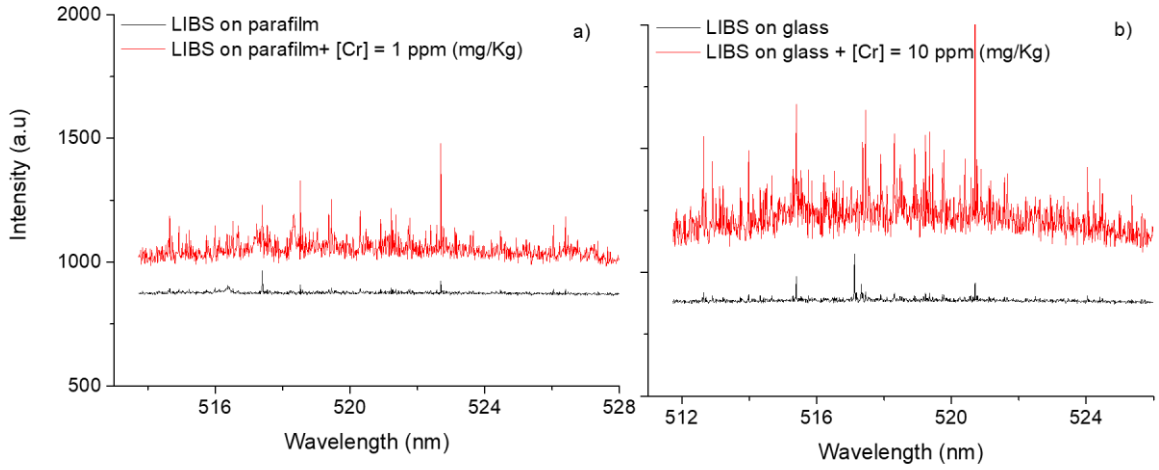

FigS6 Emission spectra during LIBS on a) parafilm and b) on glass supports, are repectively reported with and without 2 µl of Cr solution dried on the support (λ_{laser} = 532 nm, E_{laser}= 450 mJ, laser spot size = 2.2±0.2 mm, fluence = 11.84 J/cm^2; delay time = 800 ns, gate width = 10 µs, acquisition in single shot mode).

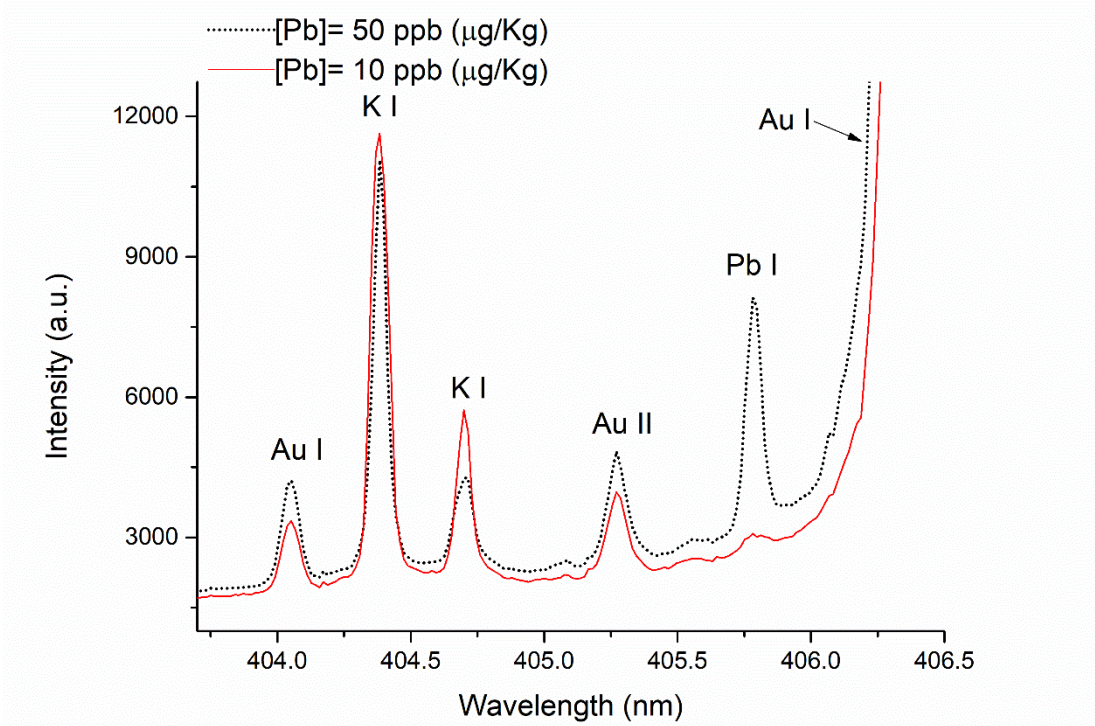

Fig. S7 Emission spectra during NELIBS of Pb solution on AuNPs-amyloids (dried on parafilm located on glass) at two different Pb concentrations: 50 and 100 ppb, respectively (λ_{laser} = 532 nm, E_{laser}= 450 mJ, laser spot size = 2.2±0.2 mm, fluence = 11.84 J/cm^2; delay time = 800 ns, gate width = 10 μs, acquisition in single shot mode).

.

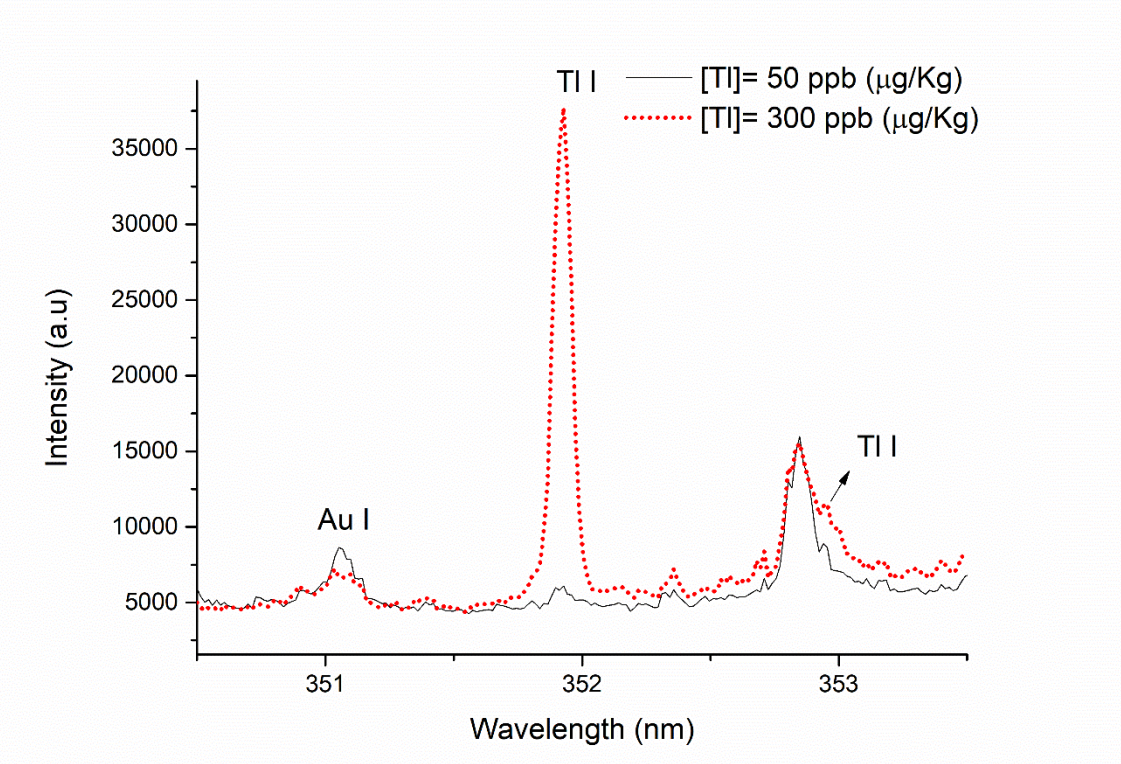

Fig. S8 Emission spectra during NELIBS of Tl solution on AuNPs-amyloids (dried on parafilm located on glass) at two different Pb concentrations: 50 and 300 ppb, respectively (λ_{laser} = 532 nm, E_{laser}= 450 mJ, laser spot size = 2.2±0.2 mm, fluence = 11.84 J/cm^2; delay time = 800 ns, gate width = 10 μs, acquisition in single shot mode).

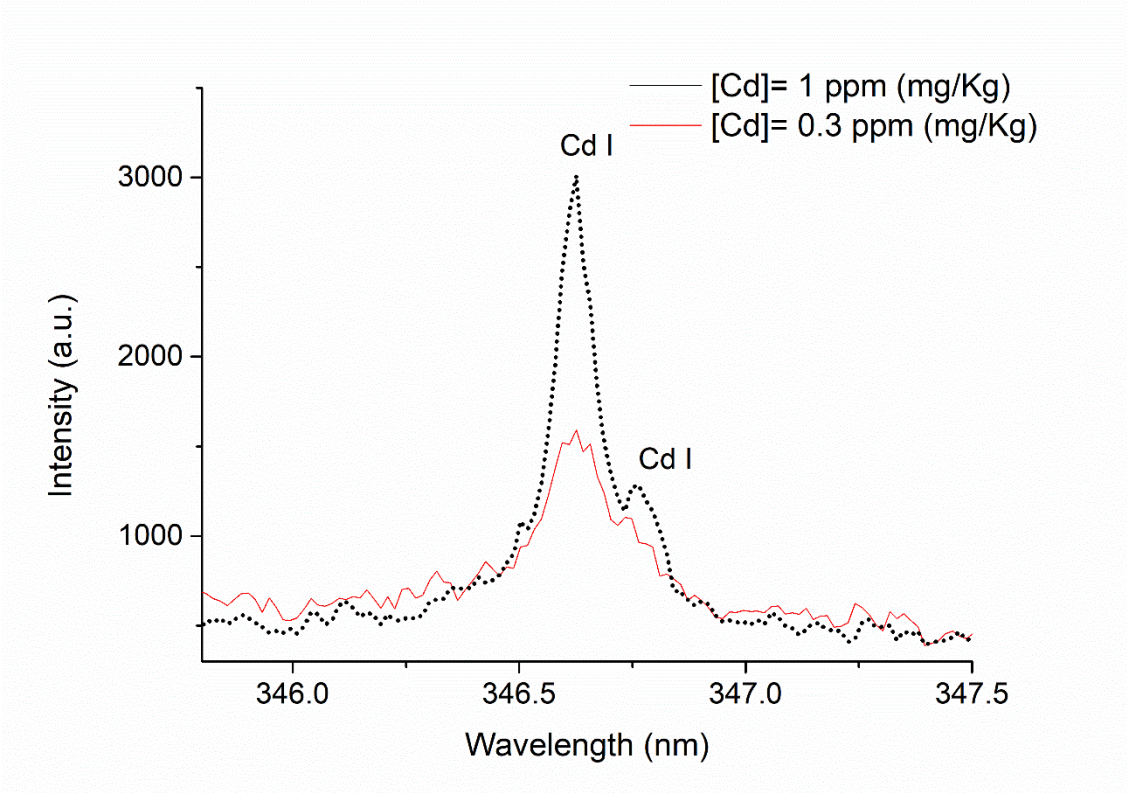

Fig. S9 Emission spectra during NELIBS of Cd solution on AuNPs-amyloids (dried on parafilm located on glass) at two different Pb concentrations: 1 and 0.3 ppm, respectively (λ_{laser} = 532 nm, E_{laser}= 450 mJ, laser spot size = 2.2±0.2 mm, fluence = 11.84 J/cm^2; delay time = 800 ns, gate width = 10 µs, acquisition in single shot mode).